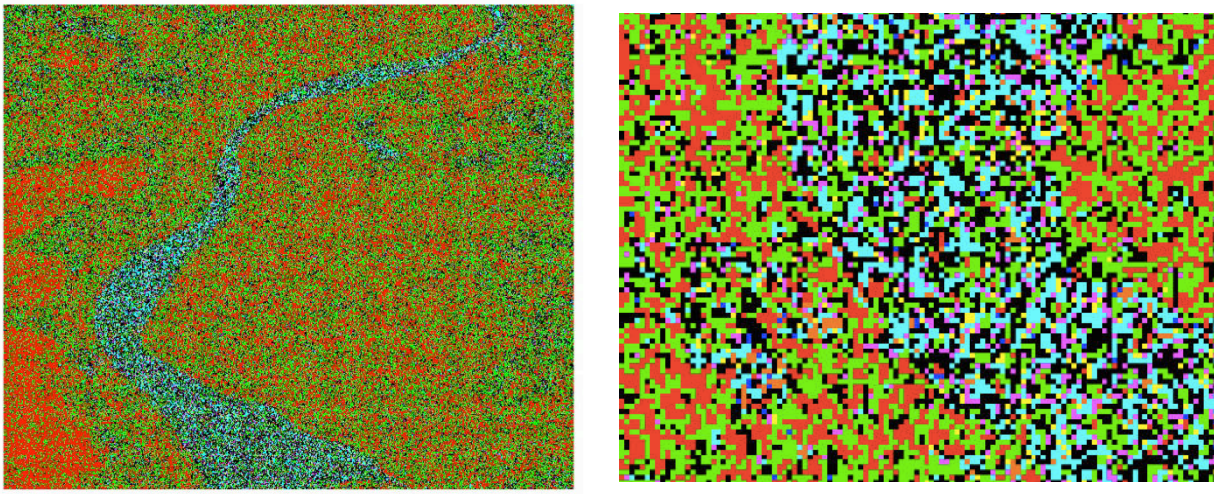

(a) **(b)**

Fig. 21. Subset A classified using H-α plane: (a) subset A, (b) area of subset A in detail

The water of the river is mainly classified as medium entropy multiple scattering zone, as well as some areas in the top right corner that also had the higher image entropy values compared with the rest of the forest. When the classified image is seen in more detail (Figure 21.b) some pinky areas appear in the river, which correspond to even higher entropy due to the randomness caused by the water surface. The general part of forest in the image is a combination of medium entropy surface scattering and low entropy surface scattering, while the crops (at the left of the image) appear more clearly as low entropy surface scattering class due to the homogeneity of the area. The regions with buildings (Figure 19) are classified as low entropy multiple scattering zones (dihedral reflectors) due to the double bounce effect of the radar wave.

- **Subset B**

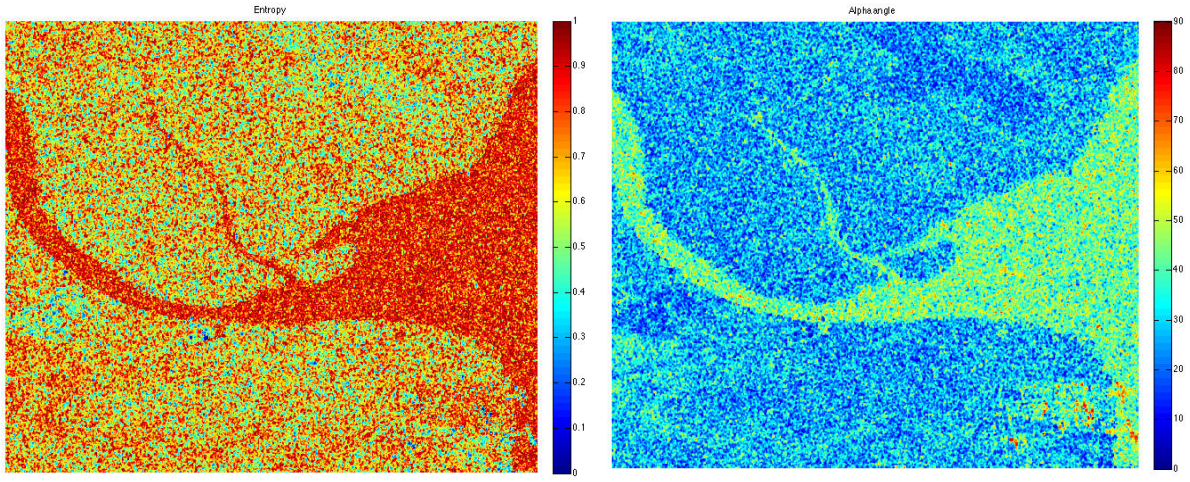

(a) **(b)**

Fig. 22. Parameters extracted from the subset B: (a) entropy, (b) alpha angle

In both Figures 22.a and 22.b the main forest and the water of the river behaves in a similar way than in the subset A; so in the water appears the highest entropy due to the smoothness of the surface causes specular reflection while in the forest there is a medium value of entropy. Unlike in subset A, near the top center and the left center of the subset B there are some forest areas with lower value of entropy, which indicates that the soil in this area is wetter so the large difference in electrical properties between water and air results in higher backscattered radar intensity. At the bottom right of subset B there is a zone with very low entropy and very high alpha referred to an area of buildings that generate a double bounce response.

The corresponding H-α plane for the subset B is represented in Figure 23.

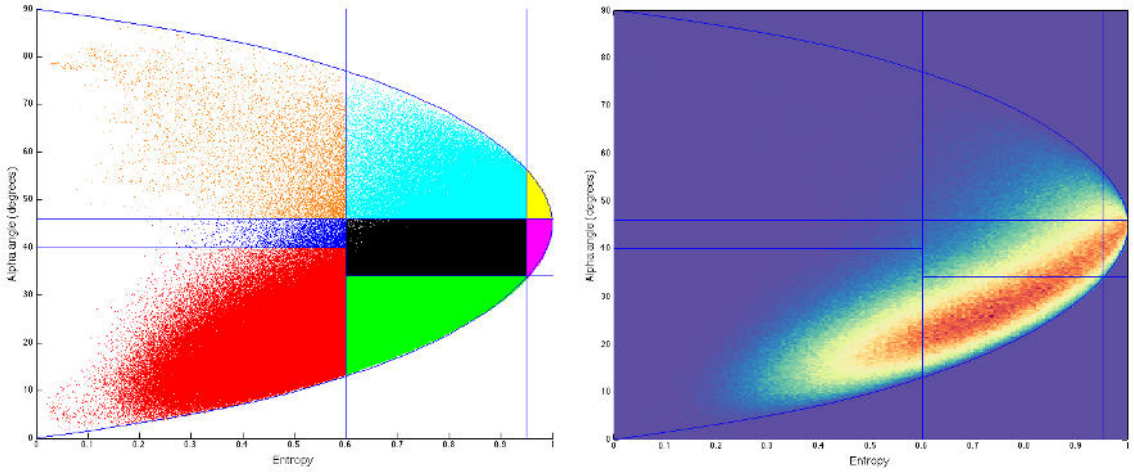

(a) **(b)**

Fig. 23. H-α plane of the subset B: (a) zones with diferent colors, (b) density plot of the plane

Both figures (23.a and 23.b) are very similar to the ones of the subset A due to the similarity of the terrain. In Figure 23.b can be appreciated that the zone 8 has more density of pixels than the set A due to the higher quantity of river.

A first classification of the subset B according to the zone to which each pixel belongs in the H-α plane is shown in Figure 24. The classification of the subset B follows a similar structure than in the subset A, so the water of the river is classified as medium entropy multiple scattering zone and the general part of forest is classified as a combination of medium entropy surface scattering and low entropy surface scattering. The previously mentioned wet areas of the forest appear more clearly as low entropy surface scattering class. The regions with buildings at the bottom right of the subset B are classified as low entropy multiple scattering zones due to the double bounce scattering mechanism at this area.

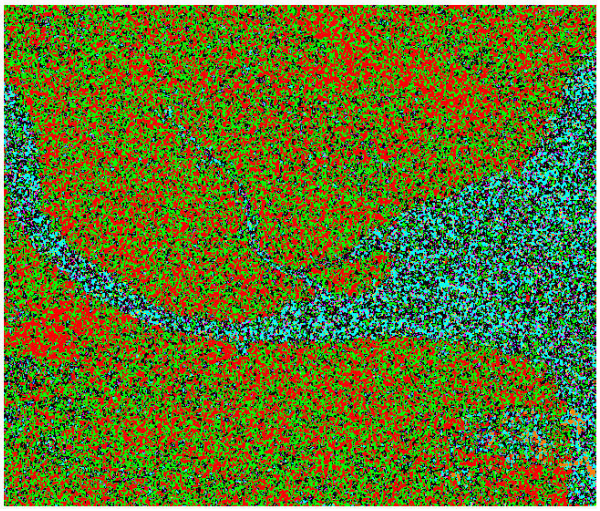

Fig. 24. Subset B classified using H-α plane

- **Subset C**

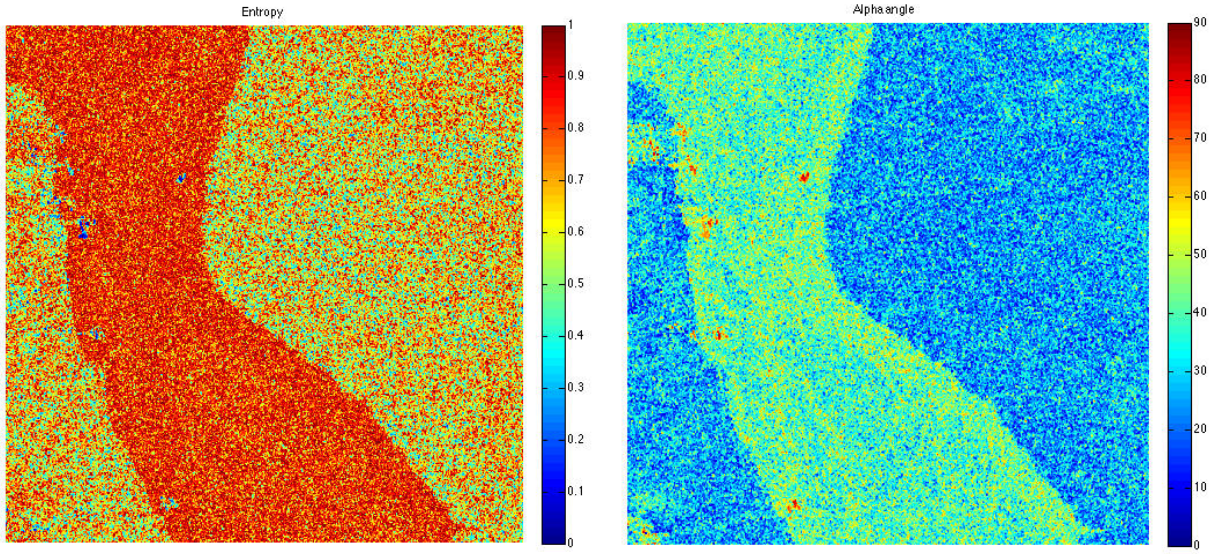

(a) **(b)**

Fig. 25. Parameters extracted from the subset C: (a) entropy, (b) alpha angle

In both Figures 25.a and 25.b the forest and the water of the river behaves again in the same way than in the subset A (in the water appears the highest entropy values while in the forest there is a medium value of entropy). There are some clearly visible ships mainly on the left side of the river that are classified as targets with very low entropy and very high alpha due to the double bounce effect of the radar wave.

The corresponding H-α plane for the subset C is represented in Figure 26. Both subfigures (Figure 26.a and Figure 26.b) are very similar to the ones of the subset A and B, although in Figure 26.b it can be appreciated that the zone 7 has more density of pixels than in the subset

B due to in this case the river, which has pixels with high entropy, occupies approximately a half part of the image.

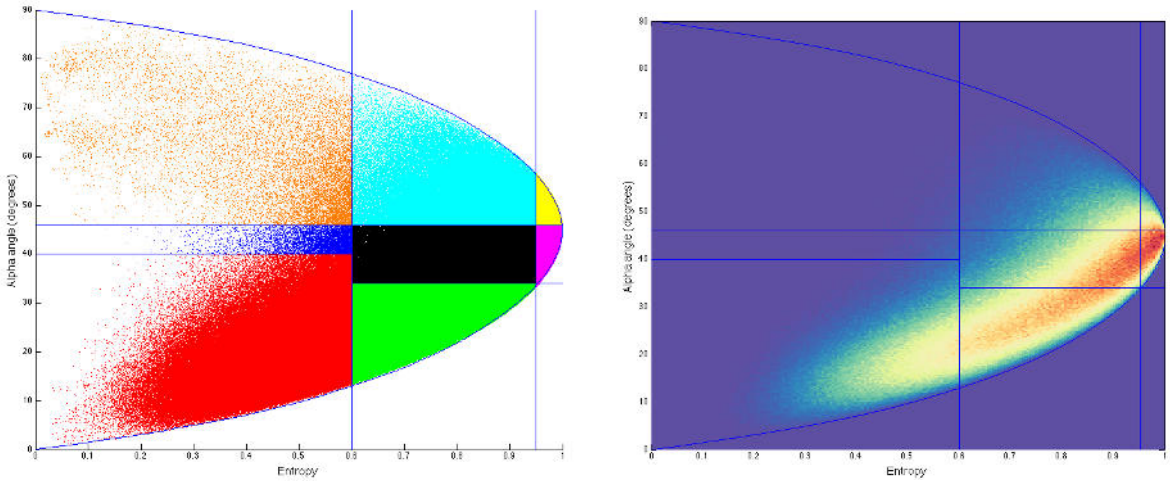

(a) **(b)**

Fig. 26. H-α plane of the subset C: (a) zones with diferent colors, (b) density plot of the plane

A first classification of the subset C according to the zone to which each pixel belongs in the H-α plane is shown in Figure 27.

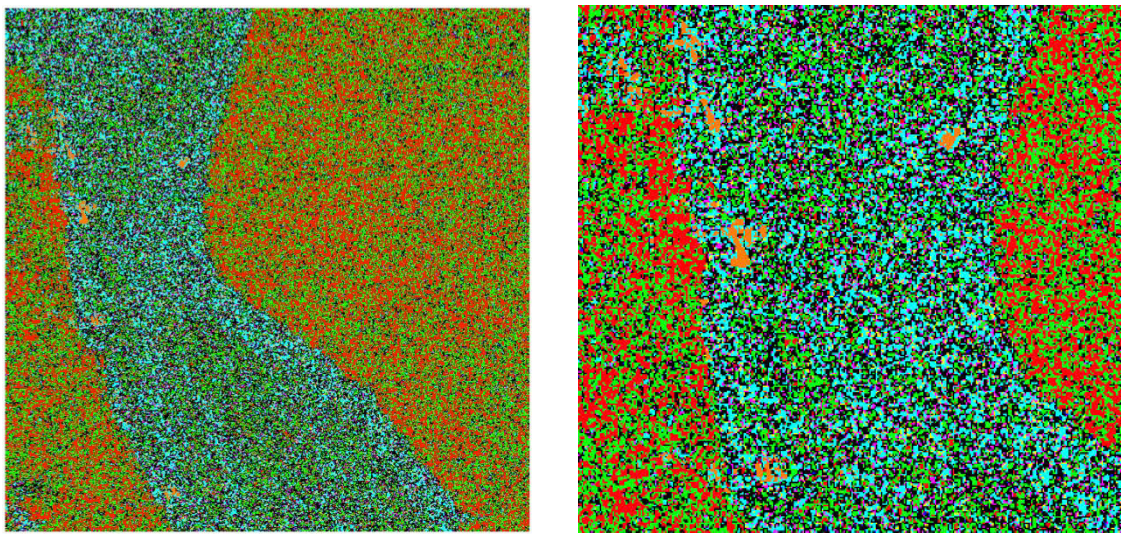

(a) **(b)**

Fig. 27. Subset C classified using H-α plane: (a) subset C, (b) area of subset C in detail

The classification of the subset C follows again a similar structure than the subset A and B, being the water of the river classified as medium entropy multiple scattering zone and the forest as a combination of medium entropy surface scattering and low entropy surface scattering. The ships on the river are easily distinguishable over the water and are clearly

classified as low entropy multiple scattering targets (dihedral reflectors) due to the generated double bounce of the wave.

These first classifications of the three subsets based on the resulting H-α plane zones of each pixel of the images give an initial idea of the different image areas, but the resulting areas mainly are a combination of two or more classes so it results in noisy classification images with heterogeneous regions. Hence, in the next Chapter a classification algorithm is going to be applied to these first classification images in order to segment more properly the initial SAR data and achieve more homogenous zones.

Chapter 6

Fuzzy clustering applied to the Case Study

6.1 Theory of Fuzzy clustering

Clustering techniques are procedures that group a set of data points in such a way that points in the same group, called a cluster, are more similar in some sense to each other than to those in other clusters and points from different clusters are dissimilar. Usually, points are in a high dimensional space and similarity is defined using a distance measure (for example Euclidean, Cosine or Jaccard) [43]. Clustering techniques are widely used in data segmentation, classification and image processing. There are two types of clustering techniques depending on the way they allocate the data points. Hard clustering is based on classical set theory, where data is divided into distinct clusters and each data element only belongs to one cluster. In fuzzy clustering, data elements can belong to several clusters at the same time, having a different degree of membership for each of them [44].

This thesis is focused in one of the most widely used fuzzy clustering algorithms, the called fuzzy c-means clustering method. This technique was originally introduced by Jim Bezdek in 1981 as an improvement on earlier clustering methods [45]. Fuzzy c-means clustering is a pretty standard least squared errors model that generalizes an earlier and very popular non- c-means model that produces hard clusters in the data. It provides a method that shows how to group data points that populate some multidimensional space into a specific number of different clusters, assigning to each of the data points several clusters with different grade of membership and iterating to move each of the clusters until they achieve a right position within the dataset.

6.1.1 Fuzzy partition

The objective of clustering is to partition a given dataset Z into c clusters. Similar to the hard partition, the fuzzy c-partitions can also be represented by partition matrices U, but allowing that the data points partially belong to different subsets with a degree of membership referred as μ_{ik}, which attain real values in [0, 1], that represents the degree to which the element i belongs to the kth sets [45].

The idea of fuzzy partitioning stems from fuzzy sets theory. A fuzzy partition includes a given number of fuzzy sets. Each set in turn includes individual elements and for these elements there are a number of grades of membership. Conditions for a fuzzy partition matrix are given by (28a), (28b) and (28c) [46]:

$$\mu_{ik} \in [0,1], \qquad 1 \le i \le c, \qquad 1 \le k \le N \tag{28a}$$

$$\sum_{i=1}^{c} \mu_{ik} = 1, \qquad 1 \le k \le N \tag{28b}$$

$$0 \le \sum_{k=1}^{N} \mu_{ik} < N, \qquad 1 \le i \le c \tag{28c}$$

The ith row of the fuzzy partition matrix U contains values of the ith membership function of the fuzzy subset A_i of Z. Depending on the value of the degree of membership μ_{ik} different cases are possible [47]:

$$\begin{cases} \mu_{ik} = 0 & i\text{th element is not a member of the } k\text{th fuzzy set} \\ \mu_{ik} = 1 & i\text{th element is a complete member of the } k\text{th fuzzy set} \\ 0 < \mu_{ik} < 1 & i\text{th element is a relative member of the } k\text{th fuzzy set} \end{cases}$$

The space of all fuzzy partitions is denoted by M_{fc} and is defined in as (29) [48].

$$M_{fc} = \left\{ U \in \mathbb{R}^{c \times N} | \mu_{ik} \in [0,1], \forall i,k; \sum_{i=1}^{c} \mu_{ik} = 1, \forall k; 0 \le \sum_{k=1}^{N} \mu_{ik} < N, \forall i \right\} \tag{29}$$

6.1.2 Fuzzy c-means Functional

In the fuzzy c-means clustering method, the objective is to minimize the sum-of-squared error or minimum variance objective function called the fuzzy c-means functional. This function represents the distance from any given data point to a cluster center weighted by that data point's membership grade and it is formulated as (30) [49]

$$J(U,V|Z) = \sum_{i=1}^{c}\sum_{k=1}^{N}(\mu_{ik})^m \|z_k - v_i\|_A^2 \tag{30}$$

where Z is a given dataset, z_k is the *i*th of d-dimensional data,

$$U = [\mu_{ik}] \in M_{fc} \tag{31}$$

is the fuzzy partition matrix of the dataset,

$$V = [v_1, v_2, \dots, v_c], \qquad v_i \in \mathbb{R}^n \tag{32}$$

is a vector of cluster prototypes (centers) that have to be determined,

$$D_{ikA}^2 = \|z_k - v_i\|_A^2 = (z_k - v_i)^T A (z_k - v_i) \tag{33}$$

is a squared inner-product distance norm expressing the similarity between any data point and the center of the cluster, where A is the norm-inducing matrix, which mainly determines the shapes of the clusters (a common choice is $A = I$, which gives the standard Euclidean norm and results in a circular shape for the clusters [50]), and

$$m \in [1, \infty) \tag{34}$$

is a parameter (*fuzziness exponent*) which significantly influences the fuzziness of the resulting clusters. If m = 1, then the partition becomes hard, that is $\mu_{ik} \in (0, 1)$ and v_i are ordinary means of the clusters. However, when $m \to \infty$, the partition becomes completely

fuzzy, that is $\mu_{ik} = 1/c$ for all i, k and the cluster means are all equal to the mean of Z. A typical value is $m = 2$.

6.1.3 Fuzzy c-means Algorithm

The fuzzy c-means algorithm solves the nonlinear optimization problem that represents the minimization of the fuzzy c-means functional doing a simple Picard iteration through the first-order conditions for stationary points of the fuzzy c-means functional [51].

The fuzzy c-means algorithm starts with an initial guess for the cluster centers, which are intended to mark the mean location of each cluster [52]. The initial guess for these cluster centers is most likely incorrect. Additionally, the fuzzy c-means algorithm assigns every data point a membership grade for each cluster. By iteratively updating the cluster centers and the membership grades for each data point, the algorithm iteratively moves the cluster centers to the right location within the dataset.

Given the dataset Z, a chosen number of clusters $1 < c < N$, the weighting exponent $m > 1$, the norm-inducing matrix A and a termination parameter ϵ; the partition matrix is initialized randomly, such that $U^0 \in M_{fc}$. The following steps of the fuzzy c-means algorithm are [50]:

- Compute the weighted means of the clusters using:

$$v_i^{(l)} = \frac{\sum_{k=1}^{N} (\mu_{ik}{}^{(l-1)})^m z_k}{\sum_{k=1}^{N} (\mu_{ik}{}^{(l-1)})^m}, \qquad 1 \le i \le c \tag{35}$$

- Compute the distances:
  for all clusters $1 \le i \le c$
  for all data objects $1 \le k \le N$

$$D_{ikA}^2 = \left(z_k - v_i^{(l)}\right)^T A \left(z_k - v_i^{(l)}\right), \qquad 1 \le i \le c, \qquad 1 \le k \le N \tag{36}$$

- Update the partition matrix:
  for all data objects $1 \le k \le N$

if $D_{ikA} > 0$ for all $i = 1,2,\dots,c$

$$\mu_{ik}{}^{(l)} = \frac{1}{\sum_{j=1}^{c}(D_{ikA}/D_{jkA})^{2/(m-1)}}, \tag{37}$$

otherwise

$$\mu_{ik}{}^{(l)} = 0 \; if \; D_{ikA} > 0 \text{ , and } \mu_{ik}{}^{(l)} \in [0,1] \text{ with } \sum_{i=1}^{c} \mu_{ik}{}^{(l)} = 1$$

until $\left\|U^{(l)} - U^{(l-1)}\right\| < \epsilon$ for some norm $\|\,.\,\|$ and for some defined ϵ.

The fuzzy c-means algorithm stops iterating when the norm of the difference between U in two successive iterations is smaller than the termination tolerance parameter ϵ. When this happens usually the partition matrix U does not significantly change anymore. Often ϵ = 0.01 or ϵ = 0.001 works well enough, depending on the trade-off between run-time and accuracy.

The fuzzy c-means algorithm converges to a local minimum of the c-means functional [53]. Hence, different initializations may lead to different results.

6.2 Application of Fuzzy clustering to the Case Study

The fuzzy c-means algorithm has been applied to the three different subsets of the Indonesia dataset. A three-dimensional space has been created to represent three parameters for each pixel of the image: its C11 element of the coherency matrix, its C22 element of the coherency matrix and its value of entropy. The off-diagonal terms of the coherency matrix are frequently ignored since they provide less amount of information. This three-dimensional space represents the data to be clustered by the algorithm, which uses as an input data a matrix for each subset where each row is a sample data point to be classified.

In order to achieve a segmentation in zones comparable with the one obtained by the H-α plane, the initial number of clusters is set to 8 ($c = 8$), which is the number of zones that provides the H-α plane according the predetermined boundaries (Table 5), and the exponent for the partition matrix U is set to 2 (m = 2). Regarding the termination criterion, the clustering process stops when the maximum number of iterations is reached (this number is initially set to 50, as it has been checked that after this number of iterations the fuzzy c-means

functional remains more constant) or when the objective function improvement between two consecutive iterations is less than the minimum amount of improvement specified.

After segmenting the input three-dimensional matrix, the partition matrix U is pseudo-colored in such a way the different segmentation zones are plotted with different colors. Taking into account that in the first step of the fuzzy c-means algorithm the partition matrix is initialized randomly and so is the class color assignation, different initializations lead to different colored results, having no correspondence the same class color within different data subsets.

Both the segmentation algorithm and the data visualization have been carry out in Matlab programming language.

6.3 Segmentation results of the Case Study

- **Subset A**

The fuzzy c-means functional is strongly minimized after the two first iterations of the fuzzy c-means algorithm during the segmentation of the subset A (Figure 28). It remains nearly constant between iterations two and five and then decreases again until iteration twelve. After this value, it remains more constant although there is a continuous minimization of the objective function, but it is difficult to appreciate due to the high steps of the axis. Fifty iterations offer a good compromise between the execution time and the segmentation results.

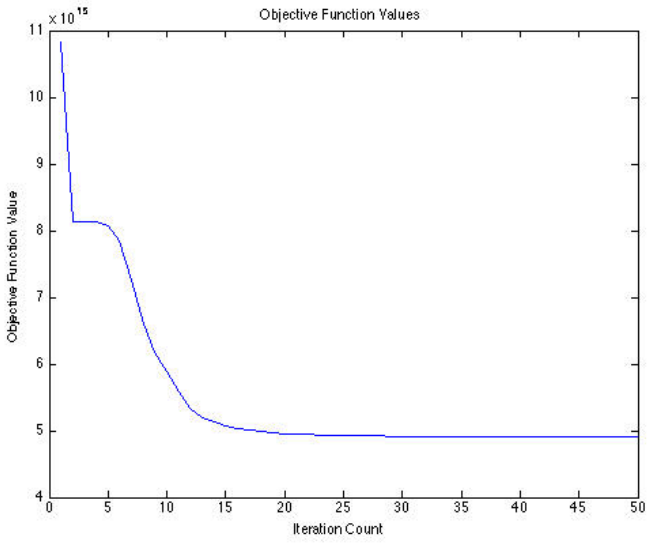

Fig. 28. Objective function values in the first 50 iterations for the subset A

The results of the subset A segmentation for different number of iterations are shown in Figure 29. After five iterations the resulting image is mainly composed by two colors, which separate the principal areas of the image, that is the silhouette of the river and the ground. After some iterations, the quality of the segmented image is highly improved; obtaining at ten iterations a visually good result and finally at fifty iterations an even better one, which has removed some apparent noise and has achieved a more homogeneous separation of the classes.

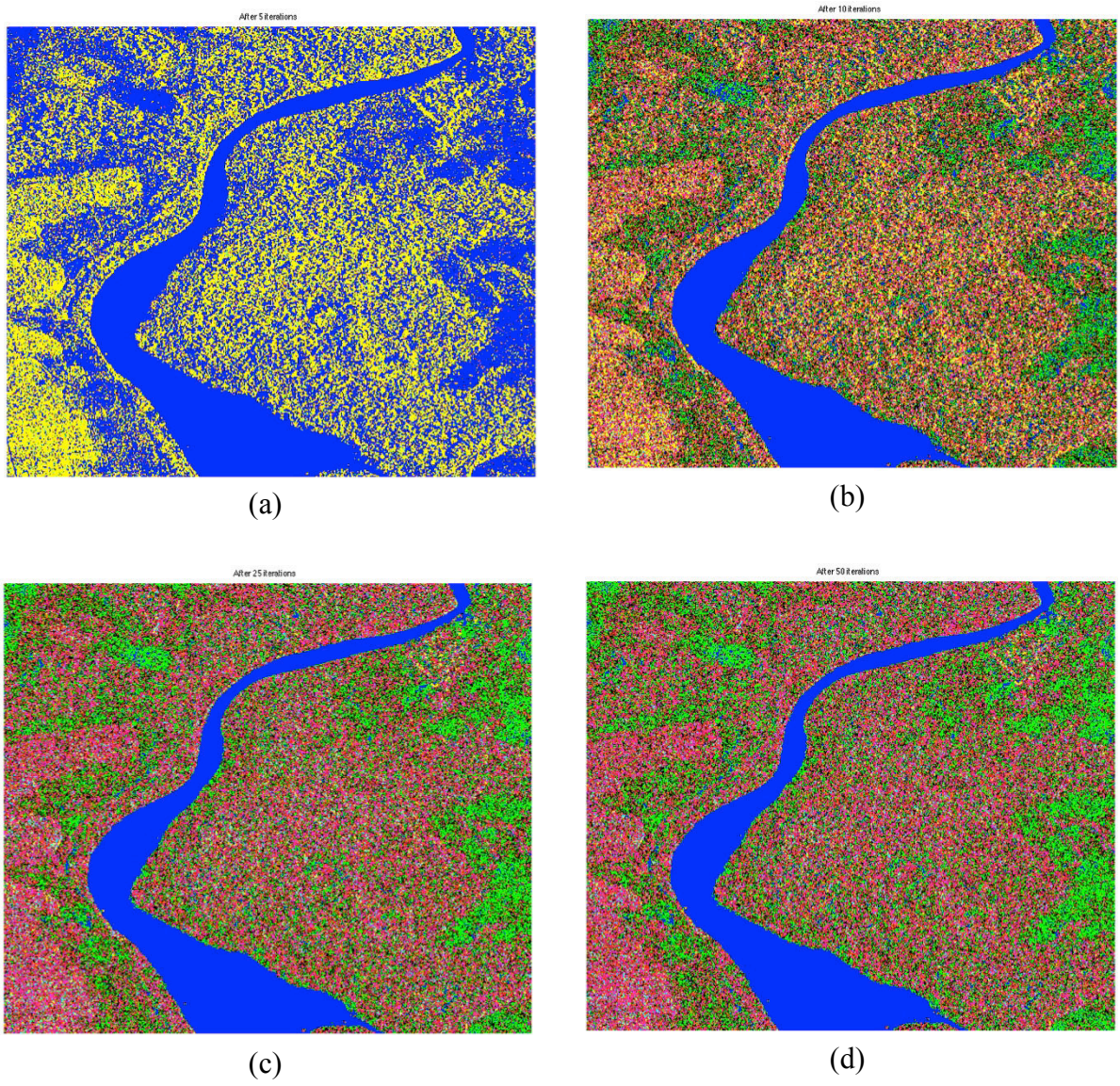

Fig. 29. Segmented and pseudo-colored image of the subset A after applying the fuzzy c-means algorithm: (a) after 5 iterations, (b) after 10 iterations, (c) after 25 iterations and (d) after 50 iterations.

The blue-colored class perfectly separates the part of the river, which corresponds to the highest entropy and the highest alpha angle area of the image. The green-colored class covers a medium-high entropy and medium alpha angle area that appears at some parts of the forest

with sparse vegetation and around the crops. There is a pinkish area at the left of the image in the zone occupied by the crops that indicates a region with the lowest values of entropy and alpha angle in the whole image. The rest of the forest, with medium entropy and medium alpha angle, is formed by a combination of different classes, mainly red, pink and green.

The segmentation of three-dimensional space formed by the entropy and the parameters C11 and C22 of the coherency matrix after applying the fuzzy c-means algorithm is shown in Figure 30, where the resulting different colored classes of the data points can be identified.

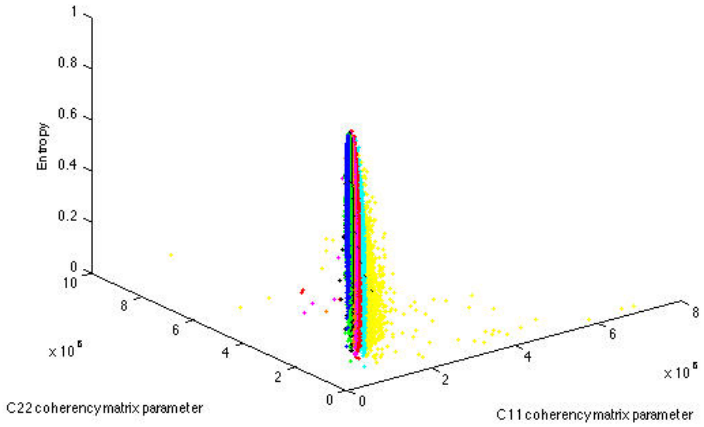

Fig. 30. Different classes obtained in the three-dimensional space after applying the fuzzy c-means algorithm in the subset A

- **Subset B**

The fuzzy c-means functional in the subset B (Figure 31) evolves in a similar way that in the subset A.

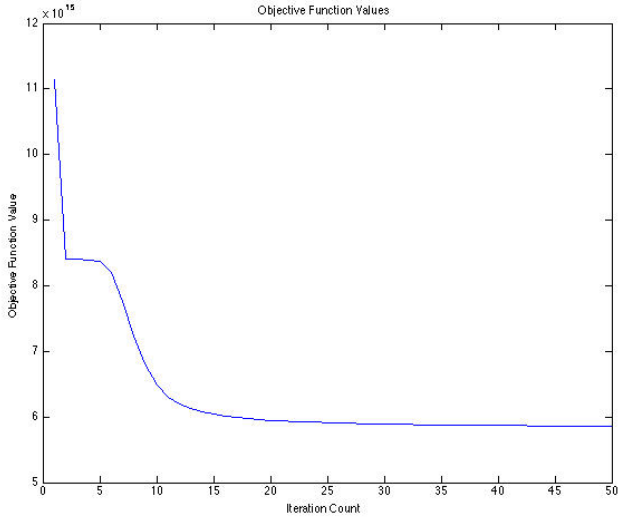

Fig. 31. Objective function values in the first 50 iterations for the subset B

Hence, it is highly minimized after the two first iterations, then it is nearly constant between iterations two and six and then decreases again until iteration twelve approximately. After this value, it remains apparently constant until iteration fifty although it has a low continuous minimization imperceptible due to the steps of the axis in the plot.

The results of the subset B segmentation for different number of iterations are shown in Figure 32. The behavior of the algorithm is similar that in the case A, so after five iterations there is a two-colored segmentation of the main areas of the image (differentiating between river and ground); after ten iterations the different classes are more perceptible and as the segmentation algorithm advances the zones become more uniform and less noisy, obtaining at fifty iterations the more homogeneous result.

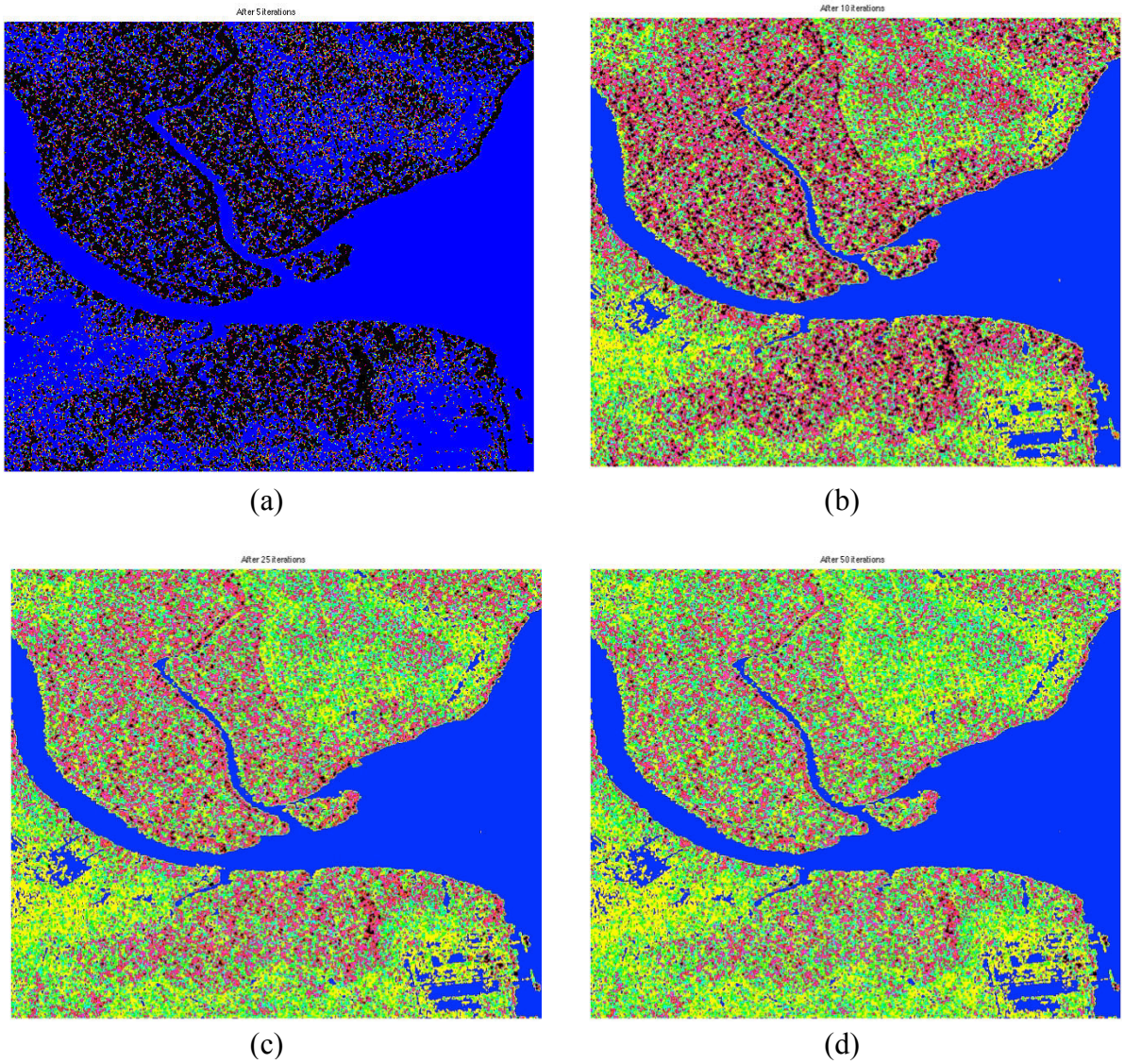

Fig. 32. Segmented and pseudo-colored image of the subset B after applying the fuzzy c-means algorithm: (a) after 5 iterations, (b) after 10 iterations, (c) after 25 iterations and (d) after 50 iterations.

The river appears homogenously segmented in the blue-class, which covers the highest entropy and the highest alpha angle area of the image. This blue-class also appears in two small areas at the bottom-left and at the bottom-right of the image due to they have a similar value of alpha angle, although the river does not occupy this area. It is noticed that there are some yellow and green-colored area at the top-right and at the bottom-left of the image that were not noticeable in the entropy and alpha images (Figure 22) but they really are in the satellite view (Figure 13.b), so the quality of the segmentation has considerably increased regarding the first H-α segmentation. The yellow-class covers medium-high entropy areas. The rest of the forest appears as a combination of pink and green colored classes, indicating areas with medium entropy and medium alpha angle. At the bottom-right corner of the image there are some clearly distinguishable ships in the river that have been well segmented.

The final colored-classes after the segmentation of three-dimensional space formed by the entropy and the parameters C11 and C22 of the coherency matrix of each image data point is shown in Figure 33.

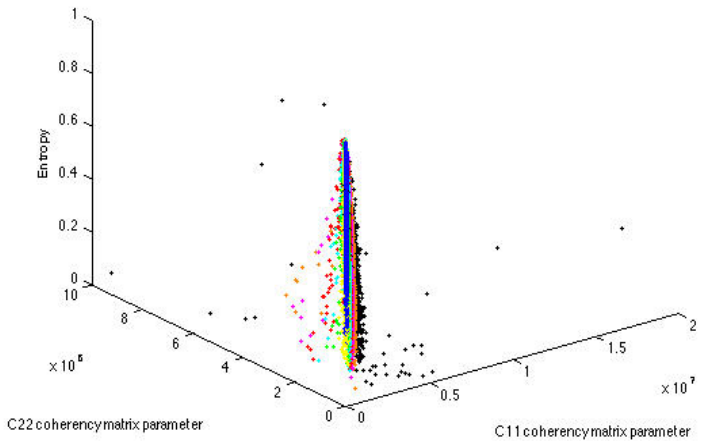

Fig. 33. Different classes obtained in the three-dimensional space after applying the fuzzy c-means algorithm in the subset B

- **Subset C**

The fuzzy c-means functional in the subset C (Figure 34) has a similar evolution than in the subset A, but it decreases stronger after the two first iterations. Then it continues nearly constant between iterations two and five. After iteration five, the objective function decreases again, but slower, until iteration twelve approximately. Finally, it remains apparently constant until iteration fifty although there is a continuous reduction of the objective function that is almost unnoticeable.

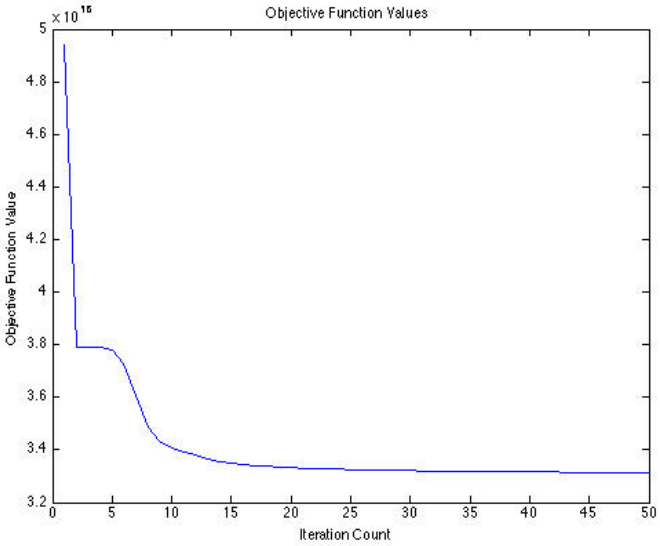

Fig. 34. Objective function values in the first 50 iterations for the subset C

The results of the subset B segmentation for different number of iterations are shown in Figure 35. As happened in the previous cases with subsets A and B, at five iterations there is a rough segmentation in the main areas in cyan and blue color, separating the river and the ground. The ships that are in the river are already noticeable at this number of iterations. At ten iterations there is a considerably good separation of classes and the different areas of the image can be differentiated. As the fuzzy c-means algorithm advances and the number of iterations is increased, the segmented image becomes more uniform and the classes are better defined, having at fifty iterations the more homogeneous result.

The river appears homogenously separated in the blue-class, representing an area with the

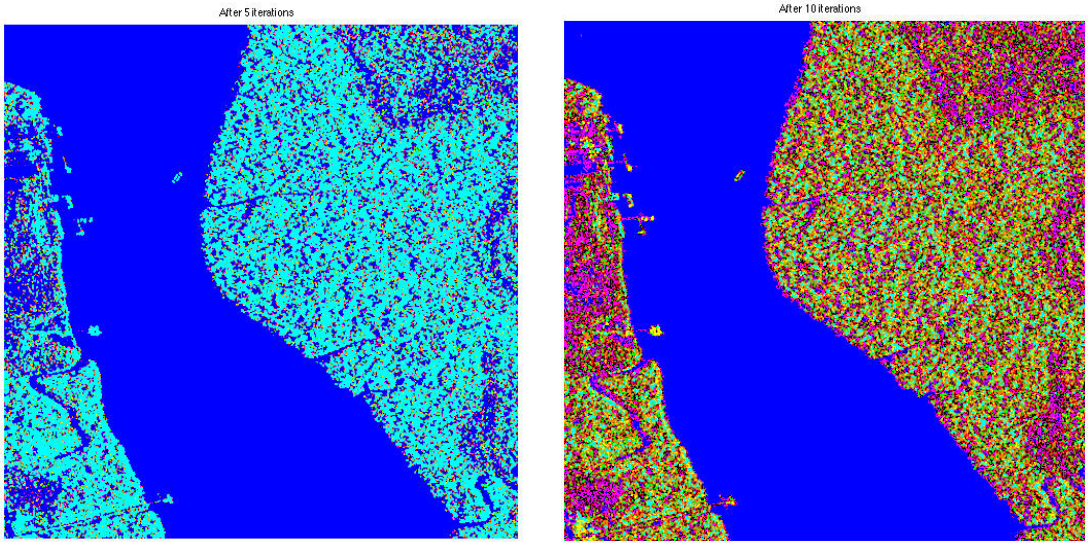

(a) (b)

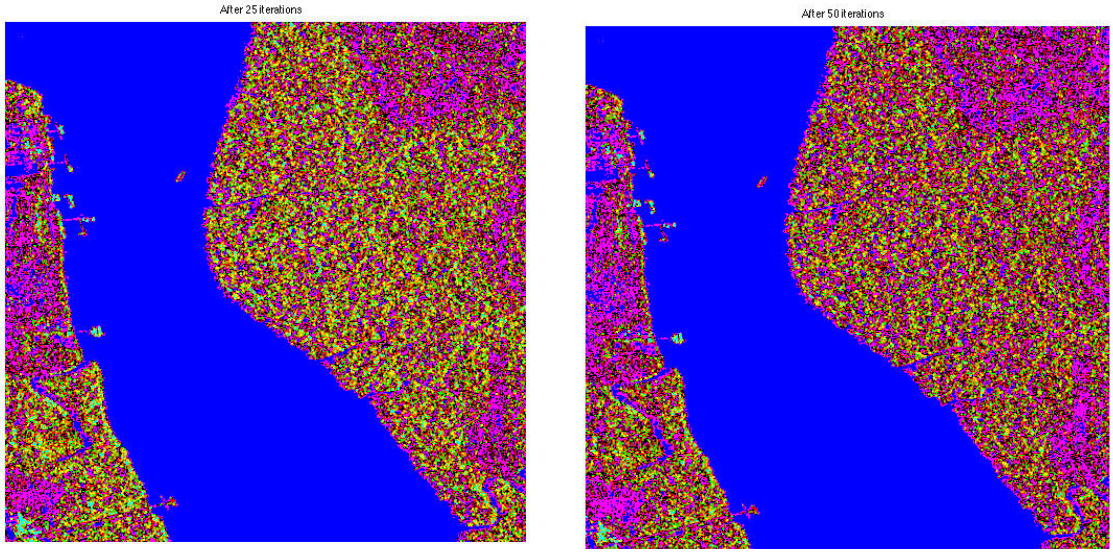

Fig. 35. Segmented and pseudo-colored image of the subset C after applying the fuzzy c-means algorithm: (a) after 5 iterations, (b) after 10 iterations, (c) after 25 iterations and (d) after 50 iterations.

highest entropy and alpha angle values. The pinkish color that appears in the forest around the image covers an area of moderated high entropy and high alpha angle; it is observed that in this case the fuzzy segmentation detects more contours and zones than the first segmentation done based on the values of entropy and alpha angle (Figure 25). The main forest appears as a combination of principally yellow and pink colors, indicating an area of medium entropy and medium alpha angle. The ships of the river, which have high alpha angle, have been well segmented and its contours are clearly distinguishable. A green-class at the bottom-left corner of the image appears at the points of high alpha angle.

The final segmentation of three-dimensional space formed by the entropy and the parameters C11 and C22 of the coherency matrix of each image data point is shown in Figure 36.

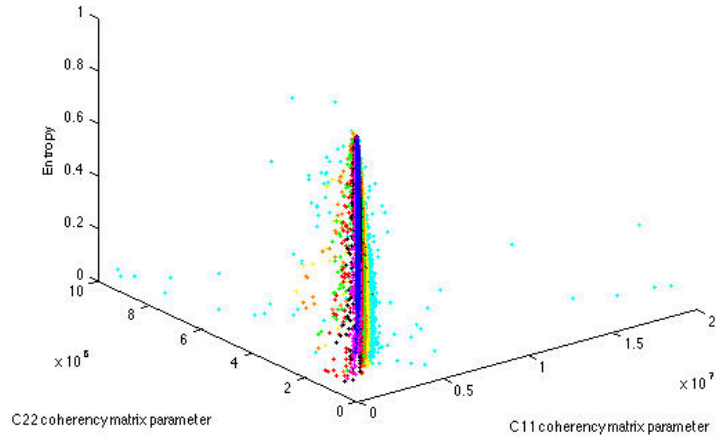

Fig. 36. Different classes obtained in the three-dimensional space after applying the fuzzy c-means algorithm in the subset C

Chapter 7

Conclusions

An unsupervised segmentation technique developed in MATLAB computing environment for dual-polarized polarimetric SAR data has been presented; using H-α theorem for data decomposition and fuzzy c-means clustering by means of entropy and diagonal coherency matrix parameters for image segmentation.

By the analysis of the H-α decomposition using TerraSAR-X dual-polarized data is concluded that entropy and alpha parameters should be considered in the polarimetric analysis, as they provide essential information about the scattering mechanisms of interaction between the incident radar wave and the target on the ground. The information in these parameters extracted by local estimation of coherency 2x2 matrix corresponds to the scattering mechanism in the pixel to be classified. It has been observed that with increasing incidence angle higher entropies are observed. This is explained by that the larger is the angle of incidence the electromagnetic wave has to go through more volume, causing it bounces more times, which generates greater disorder (high entropy). As expected, it has been obtained a high entropy value in the river region due to the specular reflection of the incident radar pulses in smooth surfaces, so very little energy is scattered back to the radar sensor.

According to the obtained results, dual-polarized SAR data, which is currently being increasingly popular, provides enough scattering information of the target to generate good segmentation results. It also offers a good trade-off between computational cost and physical knowledge of the scattering mechanisms. Dual-polarization data can be a good alternative to full-polarization data, which is linked to strong constraints in the data acquisition system and a high size of data that is difficult to manage.

The proposed image segmentation method using fuzzy c-means algorithm by means of entropy and diagonal coherency matrix parameters has generated excellent results in the areas of the image occupied by water, while the quality of the segmentation in the rest of targets has slightly decreased, though the obtained results in these parts are reasonably similar to the ones obtained with the more common segmentation methods like Wishart classifier. It has been tested that using fifty iterations of the algorithm offer a good compromise between the execution time and the segmentation results. So, due to the mentioned results in the different image areas, the whole approach exposed in this thesis could be effectively used to detect objects on the rivers surface and also could be extended to the sea.

References

[1] Inggs, M. R. and Lord, R. T., "Applications of Satellite Imaging Radar." *Department of Electrical Engineering, University of Cape Town.*

[2] Gao, G., Shi, G. and Zhou, S., "Ship Detection in High-Resolution Dual-Polarization SAR Amplitude Images." *International Journal of Antennas and Propagation*, 2013.

[3] Du, L.J. and Lee, J.S., "Polarimetric SAR image classification based on target decomposition theorem and complex Wishart distribution" *Geoscience and Remote Sensing Symposium*, Lincoln, NE, 27-31 May 1996, 439 - 441 vol.1

[4] Chan, Y. K. and Koo, V. C., "An Introduction To Synthetic Aperture Radar (SAR)" *Progress In Electromagnetics Research B*, 2008, 27-60.

[5] Tedesco, M., *Remote Sensing of the Cryosphere*. John Wiley & Sons, 2014. 12.

[6] Lee, J. S. and Pottier, E., *Polarimetric Radar Imaging: From Basics to Applications*. Boca Raton: CRC Press, 2009.

[7] Kim, A. J., Krim, A. H. and Willsky, A. S., "Segmentation-directed SAR image compression via hierarchical stochastic modeling" *AeroSense'97. International Society for Optics and Photonics, 1997,* 386-397.

[8] Atlantis Scientific Inc., "Theory of Synthetic Aperture Radar", 1997. Accessed November 8, 2014. http://www.geo.uzh.ch/~fpaul/sar_theory.html.

[9] Maini, A. K., and Agrawal, V., *Satellite Technology Principles and Applications*. 3rd ed. Chichester, West Sussex, U.K.: John Wiley & Sons, 2014. 11-15.

[10] Lakhankar, T., *Estimation of Soil Moisture Using Microwave Remote Sensing Data.* City University of New York, ProQuest, 2006.

[11] Abid, M. M., *Spacecraft Sensors*. Chichester, West Sussex, England: John Wiley & Sons, 2005. 274.

[12] Knee, P., *Sparse Representations for Radar with MATLAB® Examples*. San Rafael, Calif. (1537 Fourth Street, San Rafael, CA 94901 USA): Morgan & Claypool, 2012.

[13] Khwaja, S., *Fast Raw Data Generation of Realistic Environments for a SAR System*

Simulator. Signal and Image processing. Université Rennes 1, 2008.

[14] Reddy, M. A. *Textbook of Remote Sensing and Geographical Information Systems*. 3rd ed. Hyderabad: BS Publications, 2008. 115.

[15] Mahafza, B. R., *Radar Systems Analysis and Design Using MATLAB*. 2nd ed. Boca Raton, FL: Chapman & Hall/CRC, 2005. 534.

[16] UCL Department Of Geography, "Synthetic Aperture Radar (SAR) Summary" Accessed November 30, 2014. http://www2.geog.ucl.ac.uk/~mdisney/teaching/PPRS/PPRS_7/sar_summary.pdf.

[17] Kramer, H. J. *Observation of the Earth and Its Environment: Survey of Missions and Sensors*. 2nd ed. Berlin: Springer-Verlag, 1994. 1252.

[18] Herrmann, J. and González Bottero, A., "TerraSAR-X Mission: The New Generation in High Resolution Satellites." *Simpósio Brasileiro De Sensoriamento Remoto*, 2007, 7063-070.

[19] Christian, W., "*Radar Basics.*" Radar Tutorial. Accessed December 2, 2014. http://www.radartutorial.eu/20.airborne/ab08.en.html.

[20] Roth, A., Eineder, M. and Schättler, B., "TerraSAR-X: A New Perspective For Applications Requiring High Resolution Spaceborne Sar Data." *Commission VI, WG VI/4*.

[21] Mohanakumar, K. *Stratosphere Troposphere Interactions an Introduction*. New York: Springer, 2008.

[22] Neill, S. *Electronic Warfare and Radar Systems Engineering Handbook*. S.l.: Military Bookshop, 2013. 3-2.1.

[23] Christian, W., "Radar Basics." Polarisation of Electromagnetic Waves. Accessed December 5, 2014. http://www.radartutorial.eu/06.antennas/Polarization.en.html.

[24] Bakshi, U. A., and Bakshi, A. V., *Electromagnetic Fields*. Pune, India: Technical Publications, 2010. 40.

[25] E. Collett, "*Field Guide to Polarization*", SPIE Press, Bellingham, WA (2005).

[26] Mcnairn, H., Duguay, C., Brisco, B. and Pultz, T.j, "The Effect of Soil and Crop Residue Characteristics on Polarimetric Radar Response." *Remote Sensing of Environment*: 308-20.

[27] Natural Resources Canada, "Polarization in Radar Systems." November 13, 2014. Accessed December 23, 2014. http://www.nrcan.gc.ca/earth-sciences/geomatics/satellite-imagery-air-photos/satellite-imagery-products/educational-resources/9567.

[28] Tso, B., and Mather, P. M., *Classification Methods for Remotely Sensed Data*. 2nd ed. Boca Raton: CRC Press, 2009. 32.

[29] Karathanassi, V., and Dabboor, M., "Land Cover Classification Using E-Sar Polarimetric Data" Laboratory of Remote Sensing, School of Rural and Surveying Engineering, National Technical University of Athens, *Commission VII, WG VII/3*, 2003.

[30] Cloude, S.r., and Pottier, E., "A Review of Target Decomposition Theorems in Radar Polarimetry." *IEEE Transactions on Geoscience and Remote Sensing* 34, no. 2 (1996).

[31] Sugimoto, M. "SAR Image Analysis and Target Detection Utilizing Polarimetric Information." *National Defense Academy Graduate School of Science and Engineering*, 2013.

[32] DLR - Earth Observation. "TerraSAR-X - Germany's Radar Eye in Space." July 8, 2009. Accessed December 30, 2014. http://www.dlr.de/eo/en/desktopdefault.aspx/tabid-5725/9296_read-15979/.

[33] Ley, W. *Handbook of Space Technology*. Vol. 22. Chichester, U.K.: John Wiley & Sons, 2009.

[34] Jung, H., W. Lee, and L. Zhang. "Theoretical Accuracy of Along-Track Displacement Measurements from Multiple-Aperture Interferometry (MAI)." Sensors (Basel, Switzerland). September 23, 2014. Accessed December 29, 2014. http://www.ncbi.nlm.nih.gov/pmc/articles/PMC4208245/.

[35] LTDP Working Group. "Long Term Preservation Of Earth Observation Space Data" *European Earth Observation Space Data Set*, no. 2 (2013). Accessed December 29, 2014.

[36] Gurreonero Robinson, D. "Analysis and Evaluation in Shoreline Detection in the South Holland Province, Using Images in Quad Polarization Mode from TerraSAR-X." *Faculty of Geo-Information Science and Earth Observation of the University of Twente*, 2011.

[37] Airbus Defence and Space. "TerraSAR-X Image Product Guide." *Basic and Enhanced Radar Satellite Imagery*, no. 2 (2014).

[38] Buckreuss, S. and Schattler, B., "The TerraSAR-X Ground Segment." *IEEE Transactions on Geoscience and Remote Sensing*, no. 1.3 (2007): 623-32.

[39] Penta, B., A. O. Varghese, K. Nageswara Rao, and A. K. Joshi. "Analysis of Synthetic Aperture Radar Polarimetric Decomposition Methods for Land Cover Interpretation." *Conference: ISRS and ISG National Symposium on Remote Sensing and GIS for*

Environment with Special Emphasis on Marine and Coastal Dynamics, At Vishakhapattanam, India, 2013.

[40] Zhang, L., Zhang, J., Zou, B. and Zhang, Y., "Comparison of Methods for Target Detection and Applications Using Polarimetric SAR Image." *Harbin Institute of Technology, No. 92 West Dazhi Street, Harbin 150001, China* 4, no. 1 (2008).

[41] Theodoridis, S. and Chellappa, R., *Academic Press Library in Signal Processing Communications and Radar Signal Processing.* Vol. 2. Burlington: Elsevier Science, 2013.

[42] Sakshaug, S. E., *Evaluation of Polarimetric SAR Decomposition methods for tropical forest analysis*, Faculty Of Science And Technology, University of Tromsø, 2013

[43] Shiang, K. D. "101 Applications of Multivariate Statistical Procedures: PRINCOMP, CLUSTER, DISCRIM in SAS® 9.2." *Division of Biostatistics, Department of Information Sciences*.

[44] Miyamoto, S. and Umayahara, K., "Methods in Hard and Fuzzy Clustering." *Soft Computing and Human-Centered Machines Computer Science Workbench 2000*, 2000.

[45] Bezdek, J. C. *Pattern Recognition with Fuzzy Objective Function Algorithms*. New York: Plenum Press, 1981.

[46] Ruspini, E. H. "Numerical Methods for Fuzzy Clustering." *Information Sciences* 2, no. 3 (1970): 319-50.

[47] Azar, A., M. H. Farazmand, and A. A. A. Rostamy. "Fuzzy Partitioning And Its Application To Reservoir Operation Problem (A Multistage Approach Using Markov Chain)" *Journal of the Operations Research* 45, no. 1 (2002).

[48] Szczepaniak, Piotr S. *Fuzzy Systems in Medicine*. Vol. 41. Heidelberg: Physica-Verlag, 2000.

[49] Dunn, J. C. "A Fuzzy Relative of the ISODATA Process and Its Use in Detecting Compact Well-Separated Clusters." *Journal of Cybernetics*, 1974, 32-57.

[50] Babuška, R. "Fuzzy Clustering Algorithms." *International Series in Intelligent Technologies* 12 (1998): 49-74.

[51] Bezdek, J. C., R. Ehrlich, and W. Full. "FCM: The Fuzzy C-means Clustering Algorithm." *Computers & Geosciences* 10, no. 2-3 (1982): 191-203.

[52] Cheng, H. D., J. R. Chen, and J. Li. "Threshold Selection Based on Fuzzy C-partition Entropy Approach." *Pattern Recognition* 31, no. 7 (1997): 857-70.

[53] Czogała, E., and J. Łęski. *Fuzzy and Neuro-fuzzy Intelligent Systems*. Vol. 47. Heidelberg: Springer Science & Business Media, 2000.